International Journal of Microwave and Wireless Technologies

cambridge.org/mrf

Efficient sampling strategies based on a reduced-order model for antenna planar measurements

Valentin Morin[1], Samuel Corre[1], Renaud Loison[2], Laurent Le Coq[1] and Eric Estebe[3]

[1]Department of Ille-et-Vilaine, Univ Rennes, CNRS, IETR - UMR, Rennes, Brittany, France; [2]Department of Ille-et-Vilaine, Univ Rennes, INSA Rennes, CNRS, IETR - UMR, Rennes, Brittany, France and [3]Department of Yvelines, Thales DMS, 2 Av. Jean d'Alembert, Élancourt, Île-de-France, France

Research Paper

Cite this article: Morin V, Corre S, Loison R, Coq LL, Estebe E (2025) Efficient sampling strategies based on a reduced-order model for antenna planar measurements. *International Journal of Microwave and Wireless Technologies* **17**(6), 920–926. https://doi.org/10.1017/S1759078725000200

Received: 28 June 2024
Revised: 20 January 2025
Accepted: 29 January 2025

Keywords:
post-processing; planar near-field measurements; sampling distribution

Corresponding author: Valentin Morin;
Email: valentin.morin@univ-rennes.fr

Abstract

The antenna characterization from planar near-field (NF) measurements is generally realized by using the classical NF to far-field transform technique of plane wave expansion (PWE). This approach imposes strong constraints on NF sampling. To overcome these limitations, an equivalent model of the antenna under test (AUT) is created based on a distribution of infinitesimal dipoles. A reduced-order model (ROM) of the problem is constructed to obtain a decomposition basis defining the radiated field. The powerful ability of the ROM in determining the number of points needed for accurate NF measurements is demonstrated. Also, efficient non-conventional sampling strategies are applied to the case of planar NF measurements and the influence of these distributions on the reduction of the number of samples is studied. The global analysis of our approach on simulated and measured NF data shows that only 20% of the total number of points are needed with respect to the classical PWE technique to achieve an accurate characterization.

Introduction

The characterization of the far field (FF) radiated by an antenna under test (AUT) is crucial to verify that the radiating systems meet the expected performances. To achieve this, one way requires measuring the FF directly. Unfortunately, such measurements require quasi-plane wave illumination and are either performed at very long distances or using high-cost reflector systems. To overcome these difficulties, near-field (NF) techniques have been investigated in the second half of the last century by Hansen *et al.* [1] and Wang *et al.* [2]. The principle is based on sampling the NF before applying a near-field to far-field transform (NFFFT). The best-known NFFFT for planar measurements is the plane wave expansion (PWE) method [3], which depends on a modal expansion of the measured field. The use of Fourier transforms in this NFFFT implies that the correct identification of the decomposition coefficients is related to some sampling rules imposed by the analytical Nyquist criterion. Therefore, these rules lead to limitations on the sampling strategies that can be employed in terms of sampling distribution and size.

Many works investigated some techniques to release these constraints. A first approach developed by Bucci *et al.* [4] hinges on the use of a plane-polar sampling combined with new techniques to bring some *a priori* information on the AUT. Then, Qureshi *et al.* [5] introduce an adaptive sampling strategy to measure the NF while extrapolating it on low variations zones. Although these methods present some improvements, they are still strongly dependent on regular sampling. Therefore, the number of samples necessary to precisely characterize the AUT remains consequent, as does the measuring time.

To bypass these limits, some recent techniques propose to create an AUT model by using the Huygens, or equivalent surface, principle [4, 6]. A radiation matrix is defined to link the AUT equivalent model to the NF samples. A singular value decomposition (SVD) of this matrix leads to the construction of a reduced-order model (ROM) of the original problem.

Initially, Fuchs *et al.* [7] used this ROM approach for planar NF measurements by using a distribution of dipoles to model the AUT. The authors manage to reduce the number of samples compared to PWE for the same precision. After that, Mézières *et al.* [8] adapted it to spherical measurements for FF interpolation using the method of moments. Once again, a reduction in the number of points has been observed thanks to the conformation of the AUT geometry by the equivalent surface.

© The Author(s), 2025. Published by Cambridge University Press in association with The European Microwave Association. This is an Open Access article, distributed under the terms of the Creative Commons Attribution licence (http://creativecommons.org/licenses/by/4.0), which permits unrestricted re-use, distribution and reproduction, provided the original article is properly cited.

In this paper, a ROM is used in the case of planar NF measurements. The first objective is to demonstrate that the number of NF samples needed for accurate planar measurements can be predetermined thanks to an SVD analysis. The second objective is to show that the reduction in the number of samples can be applied to non-conventional sampling strategies.

The organization of this paper is as follows. The construction of an equivalent model of the AUT and a ROM of the problem are described in construction of a reduced-order model. The determination of the number of NF samples and the considered sampling strategies are presented in number and distribution of samples. Validations of the characterization approach with the different tools offered by the ROM are discussed in applications. The conclusion and the perspectives are provided in conclusion.

Construction of a Reduced-Order Model

Global description

As initially introduced in the context of antenna measurements by Fuchs *et al.* [7], a ROM is based on the Huygens principle, where the AUT is represented by an equivalent surface Σ [9] (Fig. 1). The equivalent currents flowing on this surface Σ can be decomposed in a known basis, created by a distribution of dipoles. Therefore, it is possible to construct a radiation matrix that links the excitations of these dipoles to the field they radiate at any observation position outside the surface Σ. For this paper, the parameter $\mathbf{E}_S$ denotes the NF measured on a surface S and $\mathbf{E}_{S'}$ the FF observed on the surface S'. Then, **A** is the radiation matrix constructed for samples on the NF planar surface S, and **A'** for observation points on S', as presented in Fig. 2.

Once the equivalent currents are computed from the measured NF $\mathbf{E}_S$, the field can be derived everywhere, in particular over S' to obtain $\mathbf{E}_{S'}$. Therefore, the proper determination of the equivalent currents is crucial to ensure a correct reconstruction $\mathbf{E}_{S'}$.

A first solution is to apply the classical sampling schemes to S to obtain regular or irregular distributions on a grid. From this NF data, the equivalent currents can be computed and used to reconstruct $\mathbf{E}_{S'}$ by solving the associated inverse problem (IP) directly.

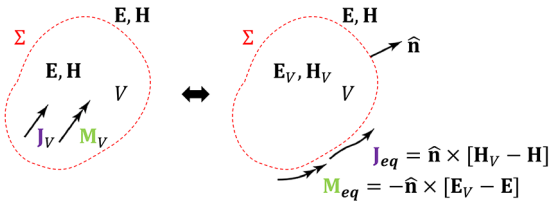


Figure 1. Illustration of the Huygens principle: (left) original problem, (right) equivalent one.

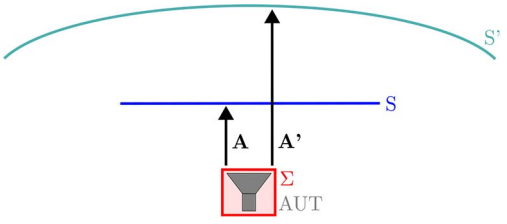


Figure 2. Matrices **A** and **A'** linking the equivalent surface Σ to the samples on the NF measurement plane S and to the observation positions on the FF half-sphere S'.

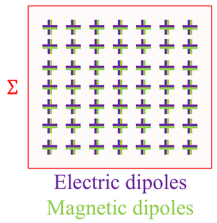


Figure 3. Distribution of infinitesimal dipoles on Σ.

Another solution is to perform an SVD of **A** constructed for a dense and regular sampling grid on S to create a ROM. The number of points to be measured can be determined and chosen among this measurement grid. Then, the equivalent currents can be computed to find $\mathbf{E}_{S'}$ or to reconstitute $\mathbf{E}_S$ on a regular grid in order to use a classical PWE to finally obtain $\mathbf{E}_{S'}$. However, the ROM can also be applied to reconstruct the regular grid for direct PWE without equivalent current determination.

Contrarily to Fuchs *et al.* [7] and Mézières *et al.* [8], our approach introduces this supplementary step of the equivalent current determination in addition to the usual ROM procedure, leading to a new ROM+IP method.

Equivalent surface discretization

The electric and magnetic equivalent currents $(\mathbf{J}_{eq}, \mathbf{M}_{eq})$ flowing on the surface Σ (Fig. 1) can be decomposed into a defined basis. In our case, the current densities $\mathbf{J}_{eq}$ and $\mathbf{M}_{eq}$ are projected on a distribution of electric and magnetic infinitesimal dipoles [11]. Two couples of crossed, tangent, dipoles (electric and magnetic) are placed along a regular grid on the equivalent surface Σ [10], as illustrated in Fig. 3. In this work, the shape of Σ is chosen square because it simplifies the problem and is well adapted to the aperture antennas that are considered in this paper. It should be noted that a more complex surface, like a box, could be used if necessary.

Construction of radiating matrices

The discretization of the equivalent surface leads to the construction of the radiation matrices **A** and **A'** by calculating the field radiated by each infinitesimal dipole on the surface Σ, at the defined points (Fig. 2). In the case of the NF measured on S, we obtain the following linear system:

$$\begin{bmatrix} \mathbf{E}_{S_x} \\ \mathbf{E}_{S_y} \end{bmatrix} = \begin{bmatrix} \mathbf{A}_{J_x} & \eta\mathbf{A}_{M_x} \\ \mathbf{A}_{J_y} & \eta\mathbf{A}_{M_y} \end{bmatrix} \begin{bmatrix} \mathbf{X}_J \\ \mathbf{X}_M \end{bmatrix} \quad (1)$$

with $\mathbf{E}_{S_x}$, $\mathbf{E}_{S_y}$ the tangential x and y components of the NF measured on S. The vectors $\mathbf{X}_J$ and $\mathbf{X}_M$ contain the weighting coefficients of the electric and magnetic currents to be determined. Thereafter, the system (1) is written $\mathbf{E}_S = \mathbf{AX}$ for more convenience. Similarly, we can compute the matrix **A'** linked to the observation positions on the surface S' and deduce the field using $\mathbf{E}_{S'} = \mathbf{A'X}$.

Inverse problem

A first method to find the equivalent currents is to solve the IP by using the least squares method $\mathbf{E}_S = \mathbf{AX}$, according to a classic sampling scheme χ on S. The resulting coefficients are the different weights associated to the dipoles on Σ. Finally, the radiated field of each dipole is used to reconstruct the FF on S' $\mathbf{E}_{S'} = \mathbf{A'X}$ (Fig. 4).

https://doi.org/10.1017/S1759078725000200 Published online by Cambridge University Press

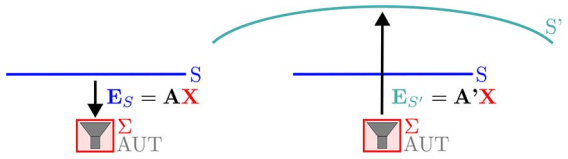


Figure 4. Steps of the IP: (left) the calculation of the equivalent currents, (right) the FF reconstruction.

Reduced-order model

A second method ROM+IP is to create a ROM of the initial problem before solving the IP. The radiation matrix $\mathbf{A}$ according to a dense regular grid $\tilde{\chi}$ on the NF surface S is constructed. It is shown in [7] that the matrices $\mathbf{A}$ and $\mathbf{A}$' are ill-conditioned because of the regularity of the currents and the redundancy of surface geometry. To get rid of this problem, an SVD of the matrix $\mathbf{A}$ is realized. This allows identifying a basis of the radiated field space and a basis of the current space. The diagonal matrix of the singular values constitutes the coupling between the two bases. The radiation matrix $\mathbf{A}$ is approximated by its truncated SVD as follows:

$$\mathbf{A} = \mathbf{USV}^H \approx \mathbf{A}_T = \mathbf{U}_T\mathbf{S}_T\mathbf{V}_T^H \tag{2}$$

with $\mathbf{U}$ and $\mathbf{V}$ two orthogonal matrices representing a radiated field basis and the associated distribution of currents on Σ, respectively. The diagonal matrix $\mathbf{S}_T$ represents the coupling of these two bases. Selecting the T first singular values boils down to only considering the T first, associated vectors of $\mathbf{U}$. The resulting matrix $\mathbf{U}_T$ represents a reduced decomposition basis of the radiated field. Furthermore, we note that the number of rows of $\mathbf{U}_T$ is directly linked to the sampling $\tilde{\chi}$.

The identification of a reduced basis in the radiated field space (2) is interesting on two points:

(i) it enables to define the minimum number of measurement points to be carried out,
(ii) it constitutes a powerful tool to interpolate the field on the surface S.

The first point will be detailed in the next section. The second one consists in selecting the number of samples determined by the ROM according to the subsampling χ defined among the points of the dense regular grid $\tilde{\chi}$ on S. From this subsampling, we can decompose the field in the reduced basis, as represented by the following system:

$$\mathbf{E}_{S_{|\chi}} = \mathbf{U}_{T_{|\chi}}\boldsymbol{\mu} \tag{3}$$

with $\mathbf{E}_{S_{|\chi}}$ and $\mathbf{U}_{T_{|\chi}}$ the measured NF and the reduced basis restricted to a subsampling χ of $\tilde{\chi}$ on the surface S, respectively. $\boldsymbol{\mu}$ is the coefficient vector associated to the decomposition of the field in the reduced basis. From the solution of the system (3), we can now interpolate the field on the dense sampling $\tilde{\chi}$: $\mathbf{E}_S = \mathbf{U}_T\boldsymbol{\mu}$. The main advantage is that the field interpolated on the dense regular measurement grid is computed from a reduced number of samples of this grid. Finally, to reconstruct the field on the surface of interest S', we solve the IP from the NF interpolated by the model.

Number and distribution of samples

From the singular values to the number of samples

As explained by Mézières *et al.* [8], the analysis of the truncated singular values matrix $\mathbf{S}_T$ by a truncation index T provides an estimation of the number of samples needed to reach an accurate characterization. This truncation index is directly dependent on a cutoff threshold R for the singular values. This threshold allows considering uniquely the singular values higher than R. The following rule is defined by the authors for spherical measurements:

$$N_{SVD} = \alpha T \tag{4}$$

with N_{SVD} the estimated number of necessary samples and α an oversampling factor equal to 1.25. Our goal is to realize the same study on the singular values to determine a safe criterion α in the case of planar NF measurements.

Sampling strategies

The introduced model allows overcoming the sampling constraints imposed by the PWE method. Indeed, we can use sampling distributions different from a regular grid respecting the Nyquist criterion, that is, with a sampling step finer than $\frac{\lambda}{2}$. In this paper, χ_{PWE} denotes these classical regular samplings. Then, the considered regular and irregular sampling strategies are the following:

(i) The regular grid with a step higher than the Nyquist criterion of $\frac{\lambda}{2}$.
(ii) The igloo sampling defined on a half-sphere by $\Delta\phi = \frac{\Delta\theta}{\sin\theta}$ [12]. This distribution created on the half-sphere is then projected by perspective from the center of Σ onto the planar measurement surface S, as illustrated Fig. 5.
(iii) With the same procedure as the igloo sampling, the Fibonacci sampling [13] is constructed on a half-sphere before being projected on S.

All these samplings can be defined as a coarse subsampling of a regular grid. This property is interesting when the ROM is applied to reconstruct $\mathbf{E}_S$ on a regular grid to use PWE because the N_{SVD} points to measure with one of the distributions previously detailed are included in the regular grid samples. From a cinematic point of view, these samplings are efficient because they do not impact

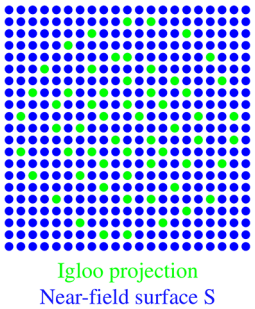


Figure 5. Perspective projection of an igloo sampling into a regular sampling over the measurement surface S.

https://doi.org/10.1017/S1759078725000200 Published online by Cambridge University Press

the path of the measurement probe relative to the classical sampling χ_{PWE}. Therefore, the acquisition time is not increasing by mechanical constraints from the measurement means. Moreover, our objective is to show that these samplings allow the reduction of the number of field samples while preserving the accuracy of the reconstructed FF.

Applications

Methodology

In this section, the first objective is to demonstrate that the number of samples needed to perform accurate NF measurements can be predetermined by an SVD analysis. The second one is to verify that non-conventional sampling strategies applied to planar NF measurements lead to a reduction in the number of samples.

In this application part, we set a square surface Σ of dimensions $5\lambda \times 5\lambda$, with a spacing between the dipoles of $\frac{\lambda}{4}$. For each AUT presented in this section, the surface Σ is positioned at the AUT aperture plane.

Metrics

For each application, a reference FF is used to measure the accuracy of both methods. We denote $\mathbf{y}$ and $\mathbf{y}_r$ respectively the reconstructed and reference FF, both calculated on each i point of the N' points over S'. Thus, the relative error associated to one polarization ($\mathbf{y}^\theta$ or $\mathbf{y}^\phi$) of the field is defined as:

$$Err_i^{\theta,\phi} = \frac{\left|\mathbf{y}_i^{\theta,\phi} - \mathbf{y}_{r_i}^{\theta,\phi}\right|}{\max\limits_{i\leq N'} \sqrt{|\mathbf{y}_r{}^\theta|^2 + |\mathbf{y}_r{}^\phi|^2}}. \quad (5)$$

In the same way, the relative error on the field modulus $Err_{mod}^{\theta,\phi}$ is defined. Then, the equivalent noise level (ENL) is introduced to evaluate the characterization accuracy:

$$ENL = \sum_{i=1}^{N'} \frac{\sqrt{\left|\mathbf{y}_i^\theta - \mathbf{y}_{r_i}^\theta\right|^2 + \left|\mathbf{y}_i^\phi - \mathbf{y}_{ri}^\phi\right|^2}}{N' \max\limits_{i\leq N'} \sqrt{|\mathbf{y}_r{}^\theta|^2 + |\mathbf{y}_r{}^\phi|^2}}. \quad (6)$$

Simulation validation – planar array at X-band

The IP and ROM+IP methods are applied to the simulated data of a 8×8 patch array working at 9.7 GHz and designed with CST MWS software [14]. The dimensions of the printed array are $4\lambda \times 4\lambda$, height 0.15λ and an array spacing of $\frac{\lambda}{2}$. The main beam direction is $\theta = 50°$ and $\phi = 0°$. The NF measurement surface over which the NF data is simulated is a square surface of dimensions $30\lambda \times 30\lambda$ positioned at a height of 4λ over the top surface of the array. The step of the sampling $\tilde{\chi}$ is set to $\frac{\lambda}{10}$ allowing to implement the various sampling strategies previously detailed. Only the x and y components of the NF are simulated and used in the IP and ROM+IP methods. The reference FF is calculated on a half-sphere according to an equi-angular sampling of $\Delta\phi = \Delta\theta = 1°$ with a limit of $\theta = 70°$ to avoid truncation effects on S.

First, we compare the reconstructions obtained by solving the IP and PWE with the CST reference for the sampling χ_{PWE} (regular, step $\frac{\lambda}{2}$) on S. The results are presented on two cut planes of S′ in Fig. 6 with the associated relative errors Fig. 7.

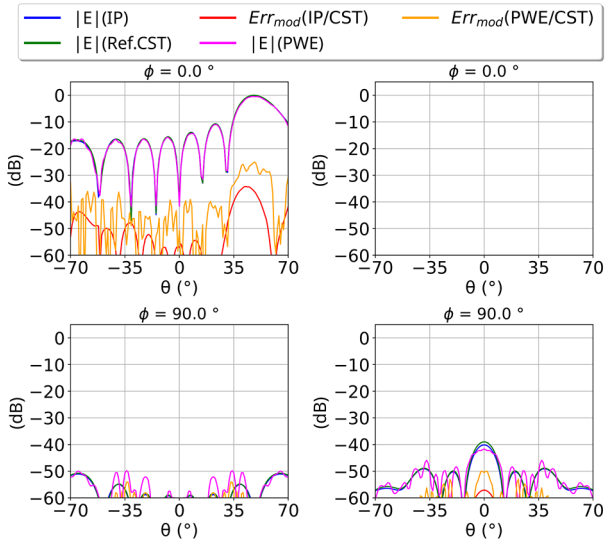


Figure 6. Patch array simulation: Comparison of the reconstructed FF by both IP and PWE methods with the sampling χ_{PWE}, relative to the reference simulated on CST. The left side focuses on the analysis of the normalized θ-component while the right side the normalized ϕ-component.

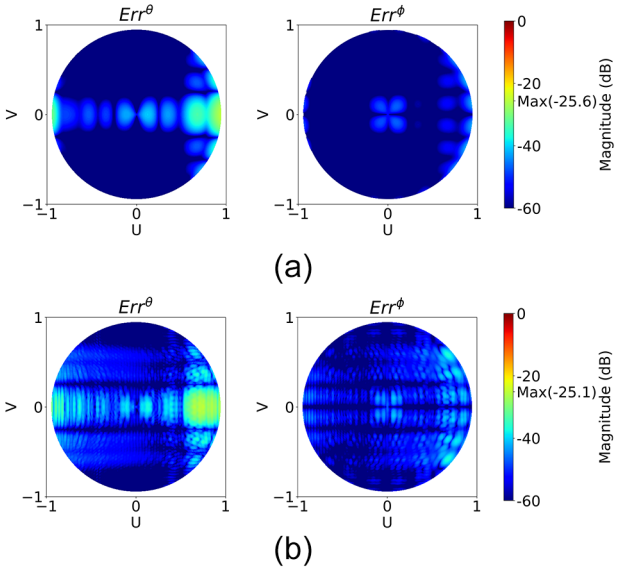


Figure 7. Patch array simulation: UV representation of the relative errors on the FF reconstruction for the two methods of IP and PWE, with the sampling χ_{PWE} on S.

The obtained results for the classical sampling χ_{PWE} show a good accuracy of the IP method compared to PWE without exploiting the ROM potential. Indeed, this is corroborated by the calculation of the *ENL* metric. For the IP, the result is −46.2 dB, while for the PWE it is −52.3 dB.

Then, the analysis of the model influence on the reconstruction accuracy by using different sampling strategies is realized in Fig. 8. The precision of characterization is studied regarding the number of samples N_χ relative to the $N_{\chi_{PWE}}$ points of the classical sampling. Moreover, the criterion N_{SVD} defined in (4) is calculated with a threshold of $R = -50$ dB. The resulting trends being stable for a

https://doi.org/10.1017/S1759078725000200 Published online by Cambridge University Press

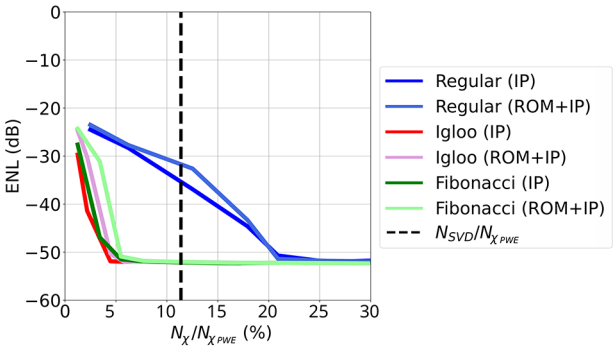


Figure 8. Patch array simulation: Methods accuracy as a function of the number of NF sampling points (relative to classical PWE sampling) and for different sampling strategies.

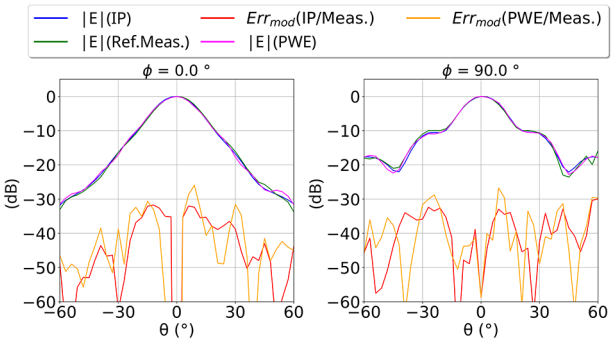


Figure 9. Pyramidal horn measurements: Comparison of the normalized co-polarization reconstructed by the IP and PWE methods with the sampling χ_{PWE}, relative to the measured FF data.

high percentage of $N_\chi/N_{\chi_{PWE}}$ points, only the variations of the *ENL* around the criterion of interest are shown.

Our approach allows an important reduction in the number of measurement points to reach the same accuracy as for the PWE. The distribution of these points on the surface S is crucial, and the irregular samplings enable us to keep only 10% of the number of samples, approximately. Also, the IP without the SVD step brings satisfactory results.

Furthermore, the oversampling factor α observed by Mézières *et al.* [8] to be equal to 1.25 in the case of spherical measurements is verified in our study for the irregular samplings. So, this criterion is still valid for a planar NF problem and ensures a safe number of points to measure according to an irregular distribution on the planar surface S. Finally, this illustrates the powerful ability of the ROM to determine the number of samples before performing the measurements.

Experimental validation – standard gain horn at V-band

The same approach is applied to the measured data of a pyramidal horn antenna working at 50 GHz [15]. The dimensions of the AUT aperture are $4\lambda \times 4\lambda$. The surface S is a square surface of dimensions $16.7\lambda \times 16.7\lambda$, at a height of 2λ from the aperture and with a sampling step of $\frac{\lambda}{3}$. This dense sampling corresponds to the $\tilde{\chi}$ sampling and also to the χ_{PWE}. Only the y component, which is the co-polarization of the NF, is measured, while the other ones are considered to be zero. The FF is calculated on the same surface S' as for the simulation case, except for the limit that is fixed in this case to $\theta = 60°$.

Now, we compare the reconstruction obtained by solving the IP and the PWE for the sampling χ_{PWE} (regular, step $\frac{\lambda}{3}$) on S with the measured FF. The results are presented in Fig. 9 without the cross-polarization because it was not measured in NF.

We can see that the characterization offered by each method is accurate compared to the measured FF. Nevertheless, the missing information on the cross-polarization from the NF measurements forces us to set the field reconstructed by PWE as the new FF reference to realize a study similar to the simulation case. Thus, the reconstruction of the model compared to this new reference, for the sampling χ_{PWE} on S, is shown in Fig. 10.

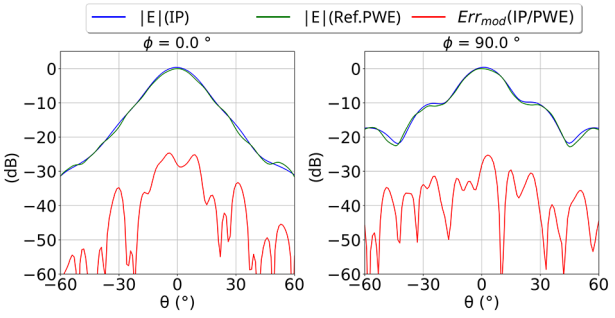


Figure 10. Pyramidal horn measurements: FF reconstruction of the normalized co-polarization from NF data measured with the sampling χ_{PWE} by solving the IP comparatively to the PWE reference.

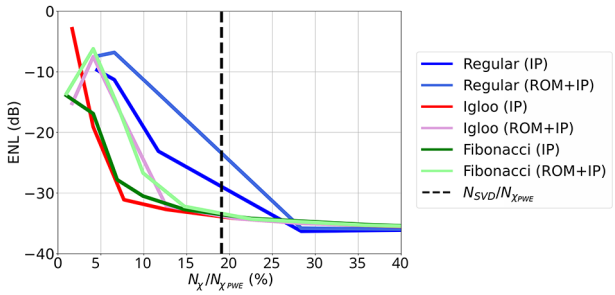


Figure 11. Pyramidal horn measurements: Methods accuracy as a function of the number of NF sampling points (relative to classical PWE sampling) and for different sampling strategies.

The analysis carried out on the IP and ROM+IP methods in the simulation case is repeated for the measured data and the results are shown in Fig. 11.

The observed trends for the simulation case are confirmed in this experimental validation. Indeed, with our approach, we need only 20% of the total number of samples compared to the PWE classical NFFFT. Moreover, the conclusion on the influence of the distribution of these points is the same: the irregular samplings are more accurate at the same number of samples than the regular one. Again, the oversampling factor of 1.25 is a good indicator of the number of samples to consider. Although the results from the ROM+IP method are slightly worse than the IP one, it is a useful tool to predict the number of measurement points. In addition, the accuracy levels achieved in this experimental case

https://doi.org/10.1017/S1759078725000200 Published online by Cambridge University Press

are higher than those observed for the simulation validation, partly because the reference is set to the FF reconstructed using the PWE method, which is marred by characterization errors. Furthermore, the measurement noises can modify the behavior of the proposed methods as well as the reference obtained by PWE method.

Conclusion

An alternative technique to the classical PWE to characterize an antenna from planar NF measurements with a low number of field samples has been presented. The creation of an equivalent model for the AUT and the construction of the associated radiation matrices have been detailed. The SVD of the NF radiation matrix associated to a dense regular grid allows the construction of a reduced decomposition basis, leading to the determination of the number of samples needed to perform a correct characterization. Then, efficient non-conventional sampling strategies enabled by the method are used to create a subsampling of the regular grid. The ROM allows retrieving the NF on a dense regular sampling over the measurement surface. Finally, FF can be obtained using equivalent current determination. The influence of the model on the characterization accuracy and the impact of the distribution of the points on the reduction of the number of samples regarding the regular grid imposed by PWE have been investigated. This analysis has been performed on simulated NF data from a planar array at X-band and also on experimental data coming from the measurement of a horn antenna at V-band. The obtained results demonstrate that the ROM oversampling criterion of 1.25 defined by Mézières *et al.* [8] is also verified for planar NF measurements with irregular samplings. The ROM is then a useful tool to estimate the number of samples when using igloo or Fibonacci samplings. It can also be applied to interpolate input NF data for the classical NFFFT technique. Moreover, efficient sampling strategies with an irregular distribution lead to an important reduction in the number of points since only 20% of the samples are necessary to ensure an accurate characterization. Finally, a global parametric study will be part of future research works to determine the influence of the model parameters on the accuracy of the characterization procedure. More particularly, it would be interesting to analyze the effects of the location of the NF samples on the measurement surface S on the reconstruction accuracy. Moreover, the extension of this work to larger antennas with strong beam tilts is currently under investigation.

Acknowledgements. This work was carried out within the framework of a ANRT funding (CIFRE contract in partnership with Thales DMS). The authors would like to thank N. Mézières for the quality of his support and the richness of his discussions. Experimental data were provided by the IETR M2ARS platform. This work is supported as part of the CPER 2021-2027 CyMoCoD project co-financed by the Ministry of Higher Education and Research, the Brittany Region, the European Union (EU-FEDER), Rennes Métropole and the Departmental Councils 35 and 22.

Competing interests. The authors declare none.

References

1. **Hansen JE** (1988) Spherical near-field antenna measurements. *IET Electromagnetic Waves Series* **26**, 8–59.
2. **Wang JJH** (1988) An examination of the theory and practices of planar near-field measurement. *IEEE Transactions on Antennas and Propagation* **36**, 746–753.
3. **Gregson SF, McCormick J and Parini C** (2007) Principles of planar near-field antenna measurements. *IET Electromagnetic Waves Series* **53**, 63–117.
4. **Bucci OM, Gennarelli C, Riccio G and Savarese C** (1998) Near-field–far-field transformation from nonredundant plane-polar data: Effective modellings of the source. *IEE Proceedings - Microwaves, Antennas and Propagation* **145**, 33–38.
5. **Qureshi MA, Schmidt CH and Eibert TF** (2012) Adaptative sampling in multilevel plane wave based near-field far-field transformed planar near-field measurements. *Progress in Electromagnetics Research* **126**, 481–497.
6. **Bucci OM, Gennarelli C, Riccio G and Savarese C** (1998) Representation of electromagnetic fields over arbitrary surfaces by a finite and nonredundant number of samples. *IEEE Transactions on Antennas and Propagation* **46**, 351–359.
7. **Fuchs B and Polimeridis AG** (2019) Reduced order models for fast antenna characterization. *IEEE Transactions on Antennas and Propagation* **67**, 5673–5677.
8. **Mézières N, Mattes M and Fuchs B** (2022) Antenna characterization from a small number of far-field measurements via reduced-order models. *IEEE Transactions on Antennas and Propagation* **70**, 2422–2430.
9. **Araque QJL and Vecchi G** (2010) Field and source equivalence in source reconstruction on 3D surfaces. *Progress in Electromagnetics Research* **103**, 67–100.
10. **Saporetti MA, Saccardi F, Foged LJ, Zackrisson J, Righero M, Giordanengo G, Vecchi G and Trenta D** (2019) Reduced sampling in NF antenna measurement using numerical defined expansion functions. *EuCAP* **13**, 1–4.
11. **Balanis C** (2016) *Antenna Theory: Analysis and Design*, 4th Edn. Hoboken, New Jersey: Wiley.
12. **Fuchs B, Le Coq L, Rondineau S and Migliore MD** (2017) Fast antenna far-field characterization via sparse spherical harmonic expansion. *IEEE Transactions on Antennas and Propagation* **65**, 5503–5510.
13. **Mézières N, Fuchs B, Le Coq L, Lerat JM, Le Fur G and Contreres R** (2020) On the application of sparse spherical harmonic expansion for fast antenna far-field measurements. *Progress in Electromagnetics Research* **19**, 746–750.
14. **CST Studio Suite** (2008) CST Microwave Studio. http://www.cst.com.
15. **Le Coq L and Fuchs B** (2014) Design and manufacturing of a high accuracy planar scanner for millimeter wave applications. *IEEE Conference on Antenna Measurements and Applications (CAMA)* 1–4.



Valentin Morin is Ph.D. student at the University of Rennes, Rennes, France. Through his thesis, he is working for the company Thales DMS on the planar near-field characterization methods of airborne active antennas with strong beam tilt.



Samuel Corre received the Ph.D. degree in Applied Mathematics from the National Institute of Applied Sciences (INSA) in 2018. He joined the Institut d'Électronique et des Technologies du numéRique (IETR) in 2021 as postdoctoral researcher for the Centre National de la Recherche Scientifique (CNRS), and became Research Engineer for the University of Rennes in 2024, where he is in charge of Softwares and Tools for Radiation Estimation, Analysis and Modeling (STREAM) facility, as member of the M2ARS (Manufacturing Measurement and Analysis of Radiating Systems) team.

https://doi.org/10.1017/S1759078725000200 Published online by Cambridge University Press



Renaud Loison is professor at the Institut National des Sciences Appliquées (INSA), Rennes, France. He carries out his research activity at the Institut d'Électronique et des Technologies du numéRique (IETR) and mainly works on antenna measurement, reflectarrays, metasurfaces and more generally on periodic and quasi-periodic surfaces.



Laurent Le Coq received the Ph.D. degree in radiocommunications in 1999 from the National Institute of Applied Science (INSA), Rennes, France. In 1999, he joined IETR (Institute of Electronics and Telecommunications of Rennes), University of Rennes 1, as a research lab engineer, responsible for antenna centi- and millimeter wave range test facilities. Since 2018, he is the scientific manager of M2ARS (Manufacturing Measurement and Analysis of Radiating Systems), the IETR facility unit bringing together seven facilities dedicated to electromagnetic studies up to 500 GHz, among which three antenna test and imaging facilities (up to 300 GHz) and a prototyping service. His activities in antenna measurements and development of related procedures involved him in more than 30 research contracts of national or European interest. He is the author and co-author of more than 50 journal papers and 50 papers in conference proceedings.



Eric Estebe graduated from Université Paul Sabatier and the Ecole Nationale Supérieure de l'Aéronautique et de l'Espace in Toulouse, France, in 1987. From 1988 to 1999, he worked in the antenna and radome department of Thomson-CSF Radar et Contre-Mesures, where he was particularly involved in the design of millimeter-wave devices and phased arrays. From 1999 to 2004, he worked at Thales Research and Technology – France on optical devices, optoelectronic modules, and technology development for microwave modules and antennas. Since 2004, he has been in charge of microwave and antenna departments involved in the development of airborne active electronically scanned arrays at Thales Defence Mission Systems. He serves as a technical referent on antennas and radiation testing.

https://doi.org/10.1017/S1759078725000200 Published online by Cambridge University Press